where K_0 is the modified Bessel function of the second kind. The Fourier transform of $f_2(\omega) = \cos \omega A_0$ is given by

$$F_2(\alpha) = \pi[\delta(\alpha - A_0) + \delta(\alpha + A_0)]. \quad \text{(A13)}$$

Using (A12) and (A13), the Fourier transform of $f_3(\omega) = f_1(\omega) f_2(\omega)$ can easily be found

$$F_3(\alpha) = K_0\left\{k_m\left(L^2 + (\alpha - A_0)^2\right)^{1/2}\right\} + K_0\left\{k_m\left(L^2 + (\alpha + A_0)^2\right)^{1/2}\right\}. \quad \text{(A14)}$$

Using (A14) in the Poisson summation formula

$$\sum_{n=-\infty}^{\infty} f_3\left(\frac{n\pi}{b}\right) = \frac{b}{\pi} \sum_{n=-\infty}^{\infty} F_3(2nb) \quad \text{(A15)}$$

after some algebraic manipulation we have

$$\sum_{n=1,2,3}^{\infty} \frac{e^{-\beta_{mn} L}}{\beta_{mn}} \left(\cos \frac{n\pi}{b}(y_1 - y_2) - \cos \frac{n\pi}{b}(y_1 + y_2)\right) = \frac{b}{2\pi} \sum_{n=-\infty}^{\infty} \left[K_0\left\{k_m\left(L^2 + (2nb - y_1 + y_2)^2\right)^{1/2}\right\} + K_0\left\{k_m\left(L^2 + (2nb + y_1 - y_2)^2\right)^{1/2}\right\} - K_0\left\{k_m\left(L^2 + (2nb - y_1 - y_2)^2\right)^{1/2}\right\} - K_0\left\{k_m\left(L^2 + (2nb + y_1 + y_2)^2\right)^{1/2}\right\}\right]. \quad \text{(A16)}$$

The modified Bessel function of the second kind decays rapidly so that, as $L \to 0$, the only significant terms in (A16) are those for $n = 0$, hence

$$\sum_{n=1,2,3,}^{\infty} \frac{e^{-\beta_{mn} L}}{\beta_{mn}} \left(\cos \frac{n\pi}{b}(y_1 + y_2) - \cos \frac{n\pi}{b}(y_1 + y_2)\right) \simeq \frac{b}{\pi}\left[K_0\left\{k_m\left(L^2 + (y_1 - y_2)^2\right)^{1/2}\right\} - K_0\left\{k_m\left(L^2 + (y_1 + y_2)^2\right)^{1/2}\right\}\right]. \quad \text{(A17)}$$

Substituting (A17) into (A9), we have

$$\sum_{m=1}^{\infty} \sum_{n=1}^{\infty} X_{mn} = -\frac{\eta_0 k_0}{\pi a} \tan\left(\frac{k_0 d_1}{2}\right) \tan\left(\frac{k_0 d_2}{2}\right) \cdot \sum_{m=1,2,}^{\infty} \left(1 - \frac{\sin^2\left(\frac{m\pi}{2a} d_1\right)}{\sin^2\left(\frac{k_0 d_1}{2}\right)}\right) \cdot \left(1 - \frac{\sin^2\left(\frac{m\pi}{2a} d_2\right)}{\sin^2\left(\frac{k_0 d_2}{2}\right)}\right) \frac{1}{k_m^2} \cdot \left[K_0\left\{k_m\left(L^2 + (y_1 - y_2)^2\right)^{1/2}\right\} - K_0\left\{k_m\left(L^2 + (y_1 + y_2)^2\right)^{1/2}\right\}\right]. \quad \text{(A18)}$$

By substituting (A8) and (A18) into (18), (20) is obtained.

REFERENCES

[1] L. Lewin, "A contribution to the theory of probes in waveguide," *Proc Inst. Elec. Eng.*, pt. C, vol. 105, pp. 109–116, 1958

[2] J. A. Bradshaw, "Scattering from a round metal post and gap." *IEEE Trans. Microwave Theory Tech*, vol. MTT-21, pp. 313–322, May 1973.

[3] S. L Lopuch and T. Koryuishii, "Field distribution of two conducting posts in a waveguide," *IEEE Trans. Microwave Theory Tech.*, vol. MTT-32, pp 29–33, Jan. 1984.

[4] O. L. El-Sayed, "Impedance characterization of a two-post mounting structure for varactor-tuned Gunn oscillators," *IEEE Trans Microwave Theory Tech.*, vol. MTT-22, pp. 769–776, Aug. 1974

[5] N Marcuvitz, *Waveguide Handbook*. New York: McGraw-Hill, ch. 5, 1951.

[6] H. Gruenberg, "Symmetrically placed inductive posts in rectangular waveguide," *Can J. Phys*, vol. 30, pp. 211–217, May 1952.

[7] K. Chang and P. J Khan, "Coupling between narrow tranverse inductive strips in waveguide," *IEEE Trans. Microwave Theory Tech.*, vol MTT-24, pp 101–105, Feb. 1976

[8] O. L. El-Sayed, "Generalized analysis of parallel two-post mounting structures in waveguide," *IEEE Trans. Microwave Theory Tech.*, vol MTT-25, pp. 24–33, Jan. 1977.

[9] J. S. Joshi and J. A. F. Cornick, "Analysis of waveguide post configurations: Part I—gap immittance matrices," *IEEE Trans. Microwave Theory Tech.*, vol. MTT-25, pp. 169–173, Mar. 1977.

[10] J. S Joshi and J. A. F. Cornick, "Analysis of waveguide post configurations: Part II—dual-gap cases," *IEEE Trans. Microwave Theory Tech*, vol. MTT-25, pp. 173–181, Mar. 1977

[11] L. Lewin, *Theory of Waveguide*. London: Newnes-Butterworths, ch 5, 1975.

[12] R. E. Collin, *Field Theory of Guided Waves*. New York: McGraw-Hill, ch. 7, Math. Appendix, 1960.

[13] R. F. Harrington, *Time Harmonic Electromagnetic Fields*. New York: McGraw-Hill, chs. 3, 7, 8, 1961.

[14] A W. Rudge, K. Milne, A. D. Olver, and P. Knight, Eds., *The Handbook of Antenna Design: Volume 2*. London: Peter Peregrinus Ltd., ch. 9, 1983.

Slow-Wave Propagation in Two Types of Cylindrical Waveguides Loaded with a Semiconductor

CLIFFORD M. KROWNE, SENIOR MEMBER, IEEE

***Abstract*—For a parallel-plate waveguide and a microstripline loaded with a semiconductor slab of resistive (or active) character, the complex propagation constant γ is determined. γ is found for higher order branches for microwave and millimeter-wave frequencies between 10 and 140 GHz, representing a study of phase velocity slowing (and attenuation).**

I. INTRODUCTION

Slow-wave structures and devices are important because of the many applications to which they have been applied and to which they may be applied in the future. Applications using an electron–electromagnetic interaction include devices such as the solid-state traveling-wave amplifier, solid-state magnetron, distributed FET, and distributed amplifier. Applications using only the electromagnetic slowing effect include the variable phase shifter, voltage-tunable filter, delay line, and variable coupling coefficient directional coupler.

It is the intent of this paper to obtain an idea of the millimeter-wave slowing behavior of cylindrical waveguide structures loaded with a semiconductor slab. To accomplish this task, two structures are examined: a parallel-plate waveguide and a microstripline, both loaded by a dielectric–semiconductor two-

Manuscript received August 16, 1983; revised November 27, 1984

The author is with the Electronics Technology Division, Naval Research Laboratory, 4555 Overlook Ave., S. W., Washington, D C. 20375-5000.

layered medium. The complex propagation constant γ is found numerically for these two structures to determine the basic attenuation and slowing properties for many branches of the dispersion diagram. The class of materials such as GaAs and InP and their related ternary and quaternary alloys are considered here (see [1] for silicon).

Due to the propagation behavior of the closed waveguide considered in this study, the isotropic resistive differential conductivity $\sigma > 0$ results also represent $\sigma < 0$ results for the same set of parameters if the real part of the propagation constant has its sign reversed when σ has its sign reversed. Thus, for a particular value of $\sigma > 0$, the low dc field microwave conductivity results may be interpreted as high dc field negative differential microwave conductivity results by merely setting the new conductivity to $-\sigma$ and reading off the propagation constants from the relevant figures with an appropriate sign reversal in the real part. This does not mean in actual practice that the high-field microwave conductivity is isotropic. The tensor nature of the microwave conductivity will certainly depend on the number of orthogonally applied dc bias electric fields. It is not within the scope of this paper to suggest specific ways of obtaining microwave conductivities less than zero at very high frequencies, which may prove to be a very difficult problem.

In the past, attention has been focused on the fundamental parallel-plate TM branch or the fundamental covered microstrip branch [2]–[5], and the fundamental coplanar line branch [6], [7], all at microwave frequencies and lower. No study of slow-wave behavior involving examination of the higher order branches at millimeter-wave frequencies has been done. This paper addresses that problem.

II. Parallel-Plate Waveguide

A. Theory

Fig. 1 shows a cross-sectional diagram of the parallel-plate waveguide structure. Medium 1 has thickness $b_1 = y_1$, complex permittivity ϵ_1', and complex permeability μ_1'. Medium 2 has thickness $b_2 = -y_2$, complex permittivity ϵ_2', and complex permeability μ_2'. By using the transverse resonance method for a transverse magnetic-field solution to the z-direction TM_z and the separation equation, one obtains

$$\gamma_i^2 + \gamma^2 + k_i^2 = 0 \tag{1}$$

and

$$\sum_i \frac{\gamma_i}{\epsilon_i'} \tanh(\gamma_i b_i) = 0 \tag{2}$$

where μ_i' and ϵ_i' are the complex permeability and permittivity in the ith medium ($i = 1$ is dielectric, $i = 2$ is semiconductor). γ_i are the transverse separation constants.

Combining (1) and (2) yields the dispersion relationship for the complex propagation constant. The dispersion equation can be written in terms of normalized variables by defining $\bar{\gamma} = \gamma/\beta_0 = \bar{\alpha} + j\bar{\beta}$ where $\beta_0 = \omega/c_0$. Here we treat a lossless dielectric medium, $\mathrm{Im}(\epsilon_1') = 0$, and a semiconductor medium 2, both layers being nonmagnetic $\mu_i' = \mu_0$ = free-space permeability. By replacing the TM_z wave impedance in (2) by the TE_z wave impedance, the transverse resonance condition for the TE_z field solution is

$$\sum_i \frac{\mu_i'}{\gamma_i} \tanh(\gamma_i b_i) = 0. \tag{3}$$

Combining (1) and (3) provides the dispersion relation for γ.

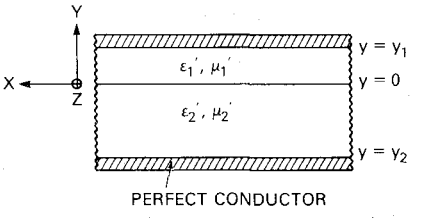

Fig. 1. Cross section of two medium loaded parallel-plate waveguide.

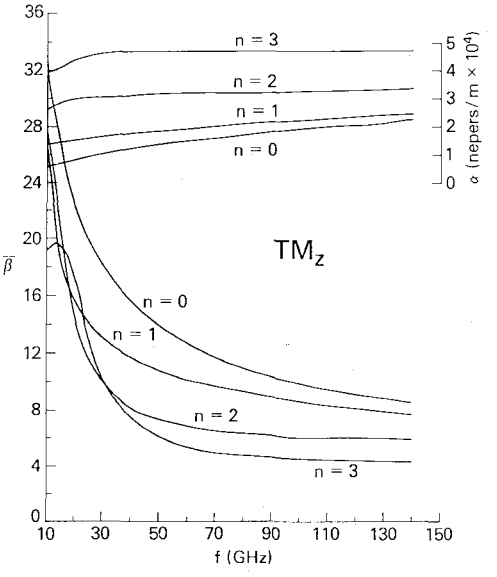

Fig. 2. α (nepers/m$\times 10^4$) and $\bar{\beta}$ versus f for TM_z parallel-plate modes. $\epsilon_{r1} = \epsilon_{r2} = 12$, $b_1 = 0.3\ \mu$m, $b_2 = 200\ \mu$m, and $\sigma = 10^3\ \mho/$m.

B. Numerical Results

Muller's method is used to determine the $\bar{\gamma} = \bar{\gamma}_n$ eigenvalue solutions to (1)–(3) where $n = 0,1,2,\cdots$ indicates the particular branch ordered according to decreasing $\bar{\beta}$, $n = 0$ being the lowest or fundamental branch with the largest slowing factor $\bar{\beta}$. The notation for n agrees with [1] (agreement with their Fig. 3 results is within 5 percent for the silicon-like system $\epsilon_{r1} = 4.5$, $\epsilon_{r2} = 12$, $b_1 = 0.3\ \mu$m, $b_2 = 190\ \mu$m, and $\sigma = 10^3\ \mho/$m) for TM_z in the $\sigma = 0$ limit, where $n = 0$ is the quasi-TEM case.

Figs. 2 and 3 give the γ results for 10 GHz $\leqq f \leqq$ 140 GHz as $\bar{\beta}$ and α versus f plotted in each figure where $\epsilon_{r1} = \epsilon_{r2} = 12$, $b_1 = 0.3\ \mu$m, $b_2 = 200\ \mu$m, and $\sigma = 10^3\ \mho/$m. Nominal values of ϵ_{ri} could correspond to depleted GaAs–GaAs layers. $\bar{\beta} > 1$ indicates phase velocity smaller than that for free space. Behavior of $\bar{\alpha}$ and $\bar{\beta}$ relative to one another may be obtained by defining a transmission Q factor as ω times the ratio of average energy in a volume section of the waveguide to average energy dissipated in the same volume, or $Q = \bar{\beta}/2\bar{\alpha}$. Evaluation of Q at 10 and 140 GHz shows that for all modes in Figs. 2 and 3, Q increases with f. For TE_z modes, the ratio $R = Q_{140}/Q_{10}$ rises with increasing branch number, being about 6 for $n = 0$ and 14 for $n = 3$. This trend indicates an improvement of the guiding structure with f in regard to losses. Such Q improvement with rising f is correlated with decreasing field penetration into medium 2 (with b_2 thickness) due to a skin-effect phenomenon. An increasing portion of the fields are contained in the lossless medium 1, as opposed to being in medium 2 at lower frequencies. At 140 GHz, $Q = 0.43$ for the TE_z $n = 0$ branch. Q values are higher for the TM_z modes, being 0.56 for the $n = 0$ branch at 140 GHz.

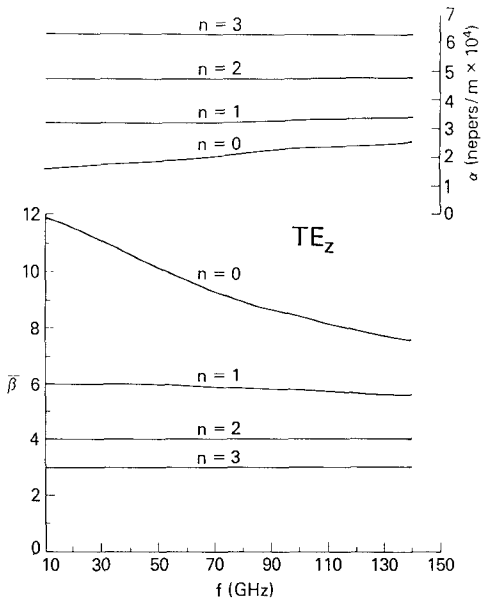

Fig. 3 α and $\bar{\beta}$ versus f for TE_z parallel-plate modes. Same parameters as in Fig. 4.

Adding electric walls at $x = \pm a$ will change the parallel-plate waveguide into a rectangular waveguide loaded with layered regions. Such a waveguide is conveniently analyzed in terms of TM_y and TE_y modes (the longitudinal section magnetic LSM and electric LSE modes). Modal solutions may be classified as even or odd according to the E_z component symmetry in the x-direction. The γ solution is

$$\gamma_{nm}^2 = \gamma_{n0}^2 + \left(\frac{m\pi}{Fa}\right)^2 \tag{4}$$

where γ_{n0} are the solutions for no wall effect. m is the order of the sinusoidal vector potential argument ($m\pi x/Fa$), with $F = 1, 2$ for, respectively, odd or even symmetry. m is an integer starting at 0 for even TM_y and odd TE_y, and at 1 for odd TM_y and even TE_y. γ_{n0} are identical to the solutions already found in Figs. 2 and 3. Setting $a = 5000$ μm, $\bar{\beta}_{nm}$ are found for $m \leqq 6$ to be slightly smaller than $\bar{\beta}_{n0}$ (by about 1 percent or less), the discrepancy becoming more noticeable as m increases.

III. Microstripline

A. Theory

Fig. 4 shows a cross-sectional drawing of the partially open microstrip structure. It has, besides the basic geometry seen in Fig. 1, electric walls placed at $x = \pm a$. These walls allow the use of a discrete Fourier transform method enabling the current distribution on the microstripline ($|x| \leqq w/2$) and the fields to be constructed from an infinite sum for the x dependence. Summation is preferable to an integral Fourier transform technique on an infinite space with oscillatory integrands requiring numerical evaluation. The sums demanding evaluation have acceptable convergence behavior. Addition of the electric walls is not unlike those discussed in Section II-B.

A superposition of the TM_z and TE_z fields in Section II-A must be used to satisfy the boundary conditions (BC) at the $y = b_1$ interface. This hybrid-mode approach is summarized below [8]. Satisfaction of the tangential BC's on E_y and E_z on the $x = \pm a$ walls is required, noting that $E_{zi}(x, y) \alpha \psi_i^{(e)}(x, y) =$ magnetic vector potential, and employing an acceptable Fourier

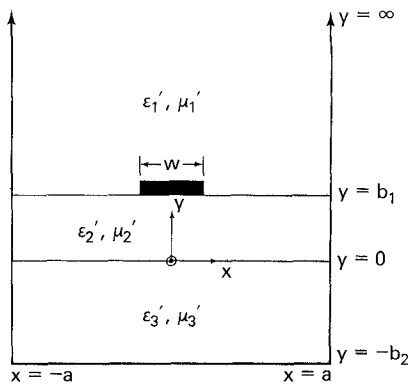

Fig. 4. Cross section of partially open microstripline.

series representation. A complete orthogonal set of exponential functions capable of representing any function $f(x)$, such as $\psi_i^{(j)}(x, y)$ on $(-a, a)$ where $j = e(TM_z)$ or $m(TE_z)$ = electric vector potential, enables the use of the following Fourier series construction and associated transform (tilde denotes transform):

$$f(x) = \frac{1}{2a} \sum_{p=-\infty}^{\infty} \tilde{f}(p) e^{-jk_p x}$$

$$= \frac{1}{a} \sum_{p=1}^{\infty} \tilde{f}(p) \begin{Bmatrix} \cos(k_p x) \\ -j\sin(k_p x) \end{Bmatrix} \tag{5}$$

$$\tilde{f}(p) = \int_{-a}^{a} f(x) e^{jk_p x}\, dx. \tag{6}$$

In the second equality of (5), the $\cos(k_p x)$ factor is used if $f(x) =$ even in x, and $\sin(k_p x)$ used if $f(x) =$ odd in x. The field solution for the microstrip problem is decomposed into two parts, the solution giving $E_{zi}(x, y)$ with even x symmetry and the solution giving E_{zi} with odd x symmetry. Even and odd solutions are obtained by respectively setting $k_p = (p - \frac{1}{2})\pi/a$, $p\pi/a$.

Surface currents exist only on the microstripline ($|x| \leqq w/2$), $J_x(x, y = b_1) = J_x(x)$, and $J_z(x, y = b_1) = J_z(x)$. They can be constructed from an infinite set of basis functions (Galerkin's method)

$$J_{x,z}(x) = \sum_{m=1}^{M,N} c_m J_{x,z;m}(x). \tag{7}$$

Finite summation limits M and N in (7) indicate truncation after a limited number of terms. Other BC's to be satisfied are $E_{x3} = E_{z2} = 0$ $(y = -b_2)$, $E_{x3} = E_{x2}$, $H_{x3} = H_{x2}$, $E_{z3} = E_{z2}$, and $H_{z3} = H_{z2}$ $(y = 0)$, and

$$H_{x,z;1}(x, b_1) - H_{x,z,2}(x, b_1) = \pm J_{z,x}(x), \qquad |x| \leqq w/2. \tag{8}$$

$\tilde{E}_{z1}$ and $\tilde{H}_{z1}$ at $y = b_1$ are found by applying all the BC's in the Fourier-transformed domain, realizing that the separation equation is

$$-k_p^2 + \gamma_i^2 + k_i^2 + \gamma^2 = 0. \tag{9}$$

In (9), γ_i are the y-direction complex propagation constants used in the formulation of the magnetic $\psi_i^{(e)}$ or electric $\psi_x^{(m)}$ potentials of the ith region in terms of hyperbolic functions (except in region 1 where they are of the form $e^{-\gamma_1 y}$).

The dispersion relationship is used here with $M = N = 1$ in (7) and is of the form

$$A_{11}^{zx}(1,1)\,A_{11}^{xz}(2,2) - A_{11}^{zz}(1,2)\,A_{11}^{xx}(2,1) = 0$$

$$A_{lm}^{jk}(l,n) = \sum_{p=1}^{L} \tilde{J}_{jl}(p)\,G_{ln}\tilde{J}_{km}(p). \tag{10}$$

Here G_{ij} are the spectral Green's function matrix elements relating electric-field tangential components to surface current components at the $y = b_1$ interface.

B. Numerical Results

To allow comparison of the numerical results to follow in this section to those in Figs. 2 and 3, the microstrip parameters are set to $\epsilon_{r1} = \epsilon_{r2} = 12$, $b_1 = 0.3$ μm, $b_2 = 200$ μm, $a = 5000$ μm, $w = 1000$ μm, and $\sigma = 10^3$ Ω/m. Because the dispersion results are not overly sensitive to the particular choice of current basis functions, and to maintain simplicity, $J_z(x)$ and $J_x(x)$ are constructed through (7) using one basis function apiece. Results for $M = N = 3$, using a complete basis function set, for example, agree with the $N = M = 1$ results to follow, to within 2 percent [1]. These basis functions are

$$J_{z1}(x) = \begin{cases} \dfrac{1}{w}, & |x| \leqq \dfrac{w}{2} \\ 0, & \dfrac{w}{2} < |x| \leqq a \end{cases} \tag{11}$$

$$J_{x1}(x) = \begin{cases} \dfrac{-j}{\pi w}\sin\left(\dfrac{2\pi x}{w}\right), & |x| \leqq \dfrac{w}{2} \\ 0, & \dfrac{w}{2} < |x| \leqq a \end{cases} \tag{12}$$

for the even modes. Basis functions for the odd modes are

$$J_{z1}(x) = \begin{cases} \dfrac{-2jx}{w^2}, & |x| \leqq \dfrac{w}{2} \\ 0, & \dfrac{w}{2} < |x| \leqq a \end{cases} \tag{13}$$

$$J_{x1}(x) = \begin{cases} \dfrac{2}{\pi w}\cos\left(\dfrac{\pi x}{w}\right), & |x| \leqq \dfrac{w}{2} \\ 0, & \dfrac{w}{2} < |x| \leqq a \end{cases} \tag{14}$$

Fig. 5 demonstrates (six even-mode branches EH_1–EH_6 are plotted) the change in γ going from a closed structure such as the parallel-plate waveguide (Fig. 1) to the partially open structure such as the microstripline (Fig. 4). (The odd-mode results are very similar.) Although for low frequencies $f \lesssim 20$ GHz decreasing $\bar{\beta}$ of the branches $EH_2, EH_3, \cdots$ corresponds to increasing α (as in Figs. 2 and 3), this progression is disrupted at higher frequencies, for example at 30 GHz. The progression is reversed beyond 40 GHz for the branches EH_1–EH_6, but this trend is not necessarily true for the other higher order modes not plotted in the figures. What appears to be occurring is that at high frequencies, say 120 GHz, the EH_1 branch wave is being guided significantly by the (open-air space)-layers combination. A wave is brought into existence which samples appreciably the air environment with some of the electromagnetic field energy lying above the $y = b_1$ interface. The effect is not as large for the EH_2 branch wave relative to the EH_1 branch wave at 120 GHz, therefore its $\bar{\beta}_2 > \bar{\beta}_1$.

Mixing of TM_y and TE_y $\bar{\beta}$ values (Figs. 2 and 3) to generate the microstripline results (Fig. 5) occurs, with a greater TE_y contribution away from the $\bar{\beta}$ peak of a branch. These peaks can

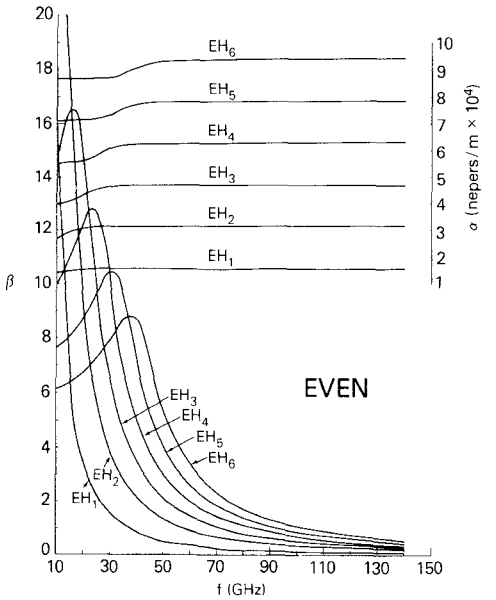

Fig. 5 α (nepers/m$\times 10^4$) and $\bar{\beta}$ versus f for even E_{zt} symmetry microstripline modes $\epsilon_{r1} = \epsilon_{r2} = 12$, $b_1 = 0.3$ μm, $b_2 = 200$ μm, $a = 5000$ μm, $w = 1000$ μm, and $\sigma = 10^3$ $\mho$/m.

be plausibly explained by referring to microstrip over a single lossless dielectric substrate. As f rises, $\bar{\beta}$ or the effective dielectric constant ϵ_{eff} rises, finally reaching ϵ_s, the substrate value. For the semiconductor loaded case at low f, a similar trend can be expected since field penetration into the semiconductor layer ought to be substantial (skin depth for Fig. 5 parameters is roughly 160 μm at 10 GHz). However, such a process cannot go on indefinitely because at large enough f, the carriers within the semiconductor will screen the field from entering a moderate portion of the layer from the overlying dielectric region (skin depth is about 43 μm at 140 GHz). The second effect will decrease ϵ_{eff} or $\bar{\beta}$ because the layers above the semiconductor have lower dielectric constants. Combination of the two above effects, acting in opposition, produces $\bar{\beta}$ peaks.

IV. Discussion

Open waveguide structures considerably reduce the slowing $\bar{\beta}$ in relation to a closed structure as demonstrated here by the microstripline and parallel-plate numerical data. If $\bar{\beta} = 8$ is taken as a measure of adequate or sizeable slowing, then this value is attained (or exceeded) over the entire 10–140-GHz range by the first two parallel-plate TM_z mode branches for the GaAs system. Only the first TE_z branch satisfies $\bar{\beta} \geqq 8$, but only up to $f \approx 110$ GHz. The other TM_z branches have $\bar{\beta} \geqq 8$ below $f \approx 39$ GHz. For the other two TE_z branches, $\bar{\beta} \geqq 8$ is never obtained. $\bar{\beta}_{EH_i}$ (even) > 8 at progressively higher i branches but with decreasing bandwidths BW, the BW being BW $= 13$ GHz when $i = 6$, centered at 37 GHz.

These results show, at least for the open microstripline, that $\bar{\beta}$ won't exceed 8 beyond about 40 GHz. $\sigma = 10^3$ $\mho$/m was chosen as a calculation value because evidence indicates a maximization of the slowing effect in the $10^3 < \sigma < 10^4$ Ω/m interval. This σ value corresponds approximately to a donor doping density N_D of 1.8×10^{16} cm^{-3} at room temperature. One expects by the proper choice of geometric parameters and σ to be able to increase $\bar{\beta}$ above the numerical data reported here for some of the branches. Validity of this supposition can be tested by calculating $\bar{\beta}$ at 100 GHz for the parallel-plate waveguide using

the following parameters: $\epsilon_{r1} = \epsilon_{r2} = 12.8$, $b_1 = 0.3$ μm, $b_2 = 25$ μm, and $\sigma = 6 \times 10^3$ $\mho$/m. Such parameters could correspond to a GaAs sample at room temperature with $N_D = 1.2 \times 10^{17}$ cm^{-3}. $\bar{\beta}$ increased from 9.24 (Fig. 2) to 20.97 with a 3.7-percent increase in α to 1.96×10^4 nepers/m. Although the $\bar{\beta}$ increase due to a change in parameters is impressive for the parallel-plate waveguide at 100 GHz, the open microstrip numerical data seen here suggest that increases of 7.4:1 and 61:1 for respectively the EH_6 and EH_1 branches are required to place $\bar{\beta}$ above 8.

Acknowledgment

The author thanks Dr. B. E. Spielman and R. E. Neidert for interesting discussions during the course of this work.

References

[1] C. M. Krowne, "Slow wave propagation in generalized cylindrical waveguides loaded with a semiconductor," *Int. J. Electron.*, to be published in 1985.

[2] H. Guckel, P. A. Brennan, and I. Palocz, "A parallel-plate waveguide approach to micro-miniaturized, planar transmission lines for integrated circuits," *IEEE Trans. Microwave Theory Tech.*, vol. MTT-15, pp. 468–476, Aug. 1967.

[3] H. Hasegawa, M. Furukawa, and H. Yanai, "Properties of microstrip line on Si-SiO_2 system," *IEEE Trans. Microwave Theory Tech.*, vol. MTT-19, pp. 869–881, Nov. 1971.

[4] J. M. Jaffe, "A high-frequency variable delay line," *IEEE Trans. Electron Devices*, vol. ED-19, pp. 1292–1294, Dec. 1972.

[5] G. W. Hughes and R. M. White, "Microwave properties of nonlinear MIS and Schottky-barrier microstrip," *IEEE Trans. Electron Devices*, vol. ED-22, pp. 945–956, Oct. 1975.

[6] R. Sorrentino and G. Leuzzi, "Full-wave analysis of integrated transmission lines on layered lossy media," *Electron. Lett.*, vol. 18, pp. 607–608, July 1982.

[7] Y. Fukuoka and T. Itoh, "Analysis of slow-wave phenomena in coplanar waveguide on a semiconductor substrate," *Electron. Lett.*, vol. 18, pp. 589–590, July 1982.

[8] T. Itoh and R. Mittra, "A technique for computing dispersion characteristics of shielded microstrip lines," *IEEE Microwave Theory Tech.*, vol. MTT-22, pp. 896–898, Oct. 1974.

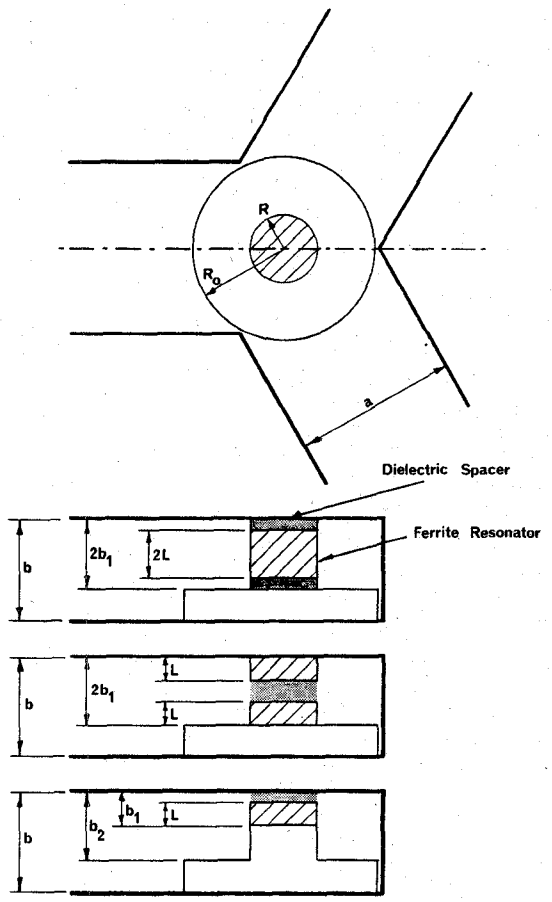

Fig. 1. Schematic diagrams of waveguide circulators using turnstile junctions.

Adjustment of In-Phase Mode in Circulators Using Turnstile Junctions

J. HELSZAJN, MEMBER, IEEE, AND J. SHARP

Abstract—**The adjustment of the counter-rotating modes of waveguide circulators using weakly magnetized turnstile junctions is fairly well understood, but some uncertainty about the definition of the in-phase mode still remains. The purpose of this paper is to remedy this situation by experimentally evaluating the in-phase eigenvalue s_0 for different filling factors and radial wavenumbers of the in-phase resonator. This is done by using the unitary condition to derive four possible relationships between the in-phase and counter-rotating eigenvalues s_0 and s_1, and the scattering variable S_{11}, and using one or another of them to form s_0. The situation for which s_0 is in anti-phase to s_1 corresponds to the first classic circulation condition of this class of device and is also derived.**

I. Introduction

The construction of the 3-port junction circulator requires the adjustment of two counter-rotating and one in-phase field patterns [1]–[3]. In the case of waveguide circulators using turnstile junctions (Fig. 1), the former ones employ quarter-wave-long resonators short-circuited at one end and open-circuited or loaded by an image wall at the other end, and the latter one usually utilizes a nearly frequency independent quasi-planar resonator which is also determined by the location of the image wall [4], [5]. The boundary conditions of the counter-rotating modes are satisfied by establishing a magnetic wall at the terminals of the junction, and that of the in-phase mode is met by placing an electric wall at the same terminals. Although the adjustment of this class of device is fairly well understood [6]–[20], there remains some uncertainty about the position of the image wall required to reconcile both boundary conditions [6], [7], [9], [10]. This difficulty is in part due to the fact that there is still no analytical description of the in-phase circuit that caters for the fringing capacitance of the resonator. The effect of a non-optimum in-phase circuit on the nature of the complex gyrator circuit of the device has been examined in [21].

The purpose of this paper is to remedy this situation by experimentally investigating the boundary condition of the in-phase circuit by using the unitary condition to derive four possible 1-port relationships between the reflection coefficient S_{11} and the phase angles of the in-phase and degenerate eigenvalues θ_0 and θ_1. One important conclusion of this work is that the filling factors of the single and coupled disk resonators' geometries are all but identical. The experimental relationship between the filling factor and radial wavenumber for both structures may therefore be represented by a single polynomial approximation. The data obtained here is in keeping with the semi-empirical upper

Manuscript received March 12, 1984; revised November 30, 1984.

J. Helszajn is with the Department of Electrical and Electronic Engineering, Heriot-Watt University, Edinburgh EH1 1HT, Scotland.

J. Sharp is with Napier College of Technology, Edinburgh, Scotland.

0018-9480/85/0400-0339$01.00 ©1985 IEEE